

# Hyperelastic behavior of porcine aorta segment under extension-inflation tests fitted with various phenomenological models

DEJAN Ž. VELJKOVIĆ<sup>1\*</sup>, VLADIMIR J. RANKOVIĆ<sup>1,2</sup>,  
SUZANA B. PANTOVIĆ<sup>3</sup>, MIRKO A. ROSIĆ<sup>3</sup>, MILOŠ R. KOJIĆ<sup>1,4</sup>

<sup>1</sup> Research and Development Center for Bioengineering BioIRC, Kragujevac, Serbia.

<sup>2</sup> Faculty of Economics, University of Kragujevac, Kragujevac, Serbia.

<sup>3</sup> Faculty of Medical Sciences, University of Kragujevac, Kragujevac, Serbia.

<sup>4</sup> The Methodist Hospital Research Institute, Houston.

Most of hyperelastic models for the constitutive modeling of the typical mechanical behaviour of the arterial wall tissue in literature are based on the test data from different animals and arteries. This paper is concerned with the material parameter identification of several phenomenological hyperelastic models by fitting the data from five extension-inflation tests of the porcine aorta segment, carried out in our laboratory. A membrane approximation is used to compute stresses and strains achieved during experiments, with usual assumption of material incompressibility. Three orthotropic two-dimensional strain-energy functions, based on use of the Green–Lagrange strains, are fitted to the test data: the well-known Fung's exponential model; the classical polynomial model with seven constants; and the logarithmic model; and also, two three-dimensional models are employed: polyconvex anisotropic exponential hyperelastic model and the convex isotropic exponential rubber-like hyperelastic constitutive law depending on the first invariant of the right Cauchy–Green deformation tensor. It has been found that isotropic model overestimates values of stresses in axial, and underestimates values of stresses in circumferential direction of artery segment, due to pronounced tissue anisotropy. Also, all two-dimensional models considered give good and similar prediction, while the polyconvex model demonstrates slightly lower performance in the axial direction of artery.

*Key words:* material parameters identification, mechanical properties, porcine aorta, strain energy function

## 1. Introduction

Passive biomechanical behaviour of arteries is nonlinear, characterized by finite deformation, anisotropy and hysteresis loop when subjected to cyclic loading and unloading. Arteries also show stress relaxation and creep. At quasi-static loading conditions, a typical mechanical behaviour of arterial wall is usually described by a hyperelastic constitutive model with appropriate type of the strain energy function (SEF) containing material parameters (constants) which are estimated by fitting the model to experimental data. There is a relatively small number of the

constitutive relations used in literature for phenomenological structural modeling of the passive mechanical response of arterial walls (Humphrey [9]). Vaishnav et al. [22] have developed two-dimensional (2D) phenomenological polynomial SEF for orthotropic incompressible arterial tissue, Fung et al. [3] proposed exponential orthotropic 2D SEF, while Takamizawa and Hayashi [21] proposed logarithmic orthotropic 2D SEF. Choung and Fung [1] also extended the well known exponential 2D model to 3D case. All these models are not convex a priori so that additional restrictions have to be imposed to material parameters, as already analyzed by Holzapfel et al. [4]; Humphrey [10]; Veljković and Kojić [24]. In contrast, Itskov et al.

\* Corresponding author: Dejan Ž. Veljković, Research and Development Center for Bioengineering, BioIRC, Prvoslava Stojanovića 6, 34000 Kragujevac, Serbia, Phone (+381) 34-500-088, e-mail: dveljkovic@kg.ac.rs

Received: June 25th, 2012

Accepted for publication: January 19th, 2014

[11] proposed a class of anisotropic (orthotropic and transversely isotropic) polyconvex exponential 3D SEFs represented by a series with an arbitrary number of terms, suitable for soft biological tissues.

Although the arterial tissue is anisotropic, isotropic models are frequently used in literature for modeling and simulations, as in Raghavan and Vorp [18] where a rubber-like polynomial SEF is used for abdominal aortic aneurysm tissue, as a function of the first invariant of the right Cauchy-Green deformation tensor, which is practically a special case of the well known Mooney-Rivlin SEFs (Mooney [14]; Rivlin and Saunders [19]). Unfortunately, this SEF is not able to capture typical stiffening effects within high pressure domain, in contrast to the isotropic exponential SEF proposed for carotid arteries by (Delfino et al. [2]), (suitable for modeling arterial walls tissue mechanical response).

All the above-mentioned phenomenological hyperelastic models treat the arterial wall as a single layer. In the literature, several multi-layer structural models were proposed based on the theory of deformation invariants, accounting for the morphological structure of the blood vessel wall, listed in the review article by Holzapfel and Ogden [8]. Strain energy function of this type (Holzapfel et al. [4]), is usually split into a part associated with isotropic deformations related to the non-collagenous ground substance, and a part associated with anisotropic deformations, related to the resistance to stretch at high pressures domain, which is almost entirely due to collagenous fibers. For modeling the isotropic contribution neo-Hookean models are used, while for modeling the anisotropic contribution, exponential functions of deformation invariants are introduced (Holzapfel and Ogden [8]). Unfortunately, it is frequent in literature that the mean fiber angle is estimated through the fitting process of the entire model, instead of separately measuring it, which can lead to unrealistic parameter estimation. Thus, although the model of Holzapfel et al. [4] is defined for the value of neo-Hookean constant  $c > 0$  (Holzapfel et al. [4]), in the papers by Holzapfel et al. [6] and Mara et al. [13] there are obtained values of  $c = 0$ , which leads to instability of the model under planar uniaxial extension, as pointed out by Veljkovic and Kojic [24]. Identification of material constants for these types of SEFs is not the topic of this paper, and could be the topic for a next study, after developing proper equipment for the mean fiber estimation in our laboratory.

For identification of SEF material parameters there are usually performed 2D experiments: planar uniaxial extension of long specimens (Raghavan and Vorp

[18]; Lally et al. [12]) and/or biaxial testing of square specimens (Sacks [20]; Lally et al. [12]; Vande Geest et al. [23]), both obtained from arterial wall and mounted in a trampoline-like fashion; or extension-inflation tests performed on the complete cylindrical segments of blood vessel, simultaneously inflated and axially extended by known force (Vaishnav et al. [22]; Fung et al. [3]; Takamizawa and Hayashi [21]).

The aim of this preliminary study is to present various, well known, phenomenological constitutive models for porcine aorta segment, together with estimated material constants obtained by fitting models to experimental data of a cylindrical segment of the porcine abdominal aorta under five extension-inflation tests (Veljković [25]). The exponential, polynomial and logarithmic 2D orthotropic SEFs; polyconvex 3D anisotropic SEF (Itskov et al. [11]), as well as the 3D isotropic exponential rubber-like hyperelastic constitutive law (Delfino et al. [2]), both depending on the invariants of the right Cauchy-Green deformation tensor, are under consideration.

Motivation for this investigation follows from the fact that hyperelastic models for constitutive modeling of typical mechanical behaviour of arterial wall tissue are usually based on the test data from different animals and/or arteries. Also, identified material constants are based on various assumptions about the thickness (membrane or thick walled assumption) of arterial tissue. All these facts do not allow proper comparisons of results obtained by using different hyperelastic SEFs, as already mentioned in [4]. For example, Vaishnav et al. [22] investigated canine aorta samples based on thick wall assumption, and proposed 2D polynomial SEF, while Fung et al. [3] observed samples of left iliac, aorta and carotid artery of rabbit, and obtained material parameters for both, polynomial and exponential SEF, based on membrane assumption. Choung and Fung [1] extended 2D model to 3D case, and fitted it to the raw data of Fung et al. [3], but now with thick-walled artery assumption. Takamizawa and Hayashi [21] introduced logarithmic SEF, and estimated material constants only for this model based on the data for the samples of dog carotid artery, also considering the artery as a thick-walled cylinder. Delfino et al. [2] performed measurements of the pressure-radius relation for different axial stretching on eight human common carotid arteries obtained fresh from autopsy. The values of material parameters of their isotropic exponential model are given, but without any details of tests performed and assumptions used. Raghavan and Vorp [18] introduced a simple isotropic constitutive law based only on planar uniaxial tests data of human abdominal aor-

tic aneurysm tissue specimens, while Lally et al. [12] accomplished series of uniaxial and equibiaxial tension tests on healthy porcine coronary arteries, and fitted obtained data with one form of the Mooney–Rivlin rubber-like SEF. Vande Geest et al. [23] performed series of planar tension control biaxial tests on square human samples of aneurysmal and nonaneurysmal abdominal aortic tissue, and fitted obtained data to one form of 2D orthotropic exponential model. Itskov et al. [11] proposed a new form of exponential polyconvex 3D SEF, and tested it by fitting to the raw data of bovine pericardium and fitted data of rabbit skin, both obtained from literature.

In the next section we start by reviewing the elastic constitutive law of an incompressible hyperelastic material. Next, we outline the form of the constitutive relations for exponential, logarithmic and polynomial 2D orthotropic models, polyconvex anisotropic 3D model, and exponential isotropic 3D model. Then, the experimental setup is discussed, together with the description of strains and related stresses, and formulas used in the analysis. The observed experimental data are presented. After that, the fitted material parameters are given as well as the graphical comparison of the results obtained for the three representative protocols and the values given by stress-strain relationships corresponding to the exponential 2D model, and the isotropic and anisotropic 3D models.

## 2. Materials and methods

### 2.1. Basic equations and hyperelastic models

The second Piola–Kirchhoff stress tensor  $\mathbf{S}$ , for an incompressible hyperelastic material, characterized by a three-dimensional SEF  $\psi = \psi(\mathbf{E})$  expressed in terms of components of the Green–Lagrange strain tensor  $\mathbf{E} = (\mathbf{C} - \mathbf{I})/2$  is given by

$$\mathbf{S} = -p\mathbf{C}^{-1} + \frac{\partial\psi}{\partial\mathbf{E}}, \quad (1)$$

together with the incompressibility constraint

$$\det \mathbf{C} = \det(\mathbf{I} + 2\mathbf{E}) = 1. \quad (2)$$

Here,  $\mathbf{I}$  denotes the second order unit tensor,  $\mathbf{C} = \mathbf{F}^T \mathbf{F}$  denotes the right Cauchy–Green deformation tensor, and  $\mathbf{F}$  is the deformation gradient tensor. The scalar  $p$  is identified as a hydrostatic pressure, and may be

obtained only from the equilibrium equations and the boundary conditions (Holzapfel [5]; Ogden [15]).

In order to characterize mechanical properties of the incompressible arterial wall material, 2D formulation is often used (Holzapfel et al. [4]), which is not capable of fully describing 3D anisotropic behavior of a thick-walled cylindrical tube under, for example, combined inflation and torsion. For the 2D theory, SEF depends only on the in plane deformation components  $E_{11}$ ,  $E_{22}$ ,  $E_{12}$  and the corresponding stresses are given as (Holzapfel and Ogden [7])

$$S_{11} = \frac{\partial \hat{\psi}}{\partial E_{11}}, \quad S_{22} = \frac{\partial \hat{\psi}}{\partial E_{22}}, \quad S_{12} = \frac{\partial \hat{\psi}}{\partial E_{12}}. \quad (3)$$

Here,  $\hat{\psi} = \hat{\psi}(E_{11}, E_{22}, E_{12})$  denotes an *a priori* 2D hyperelastic strain energy function.

The well-known 2D hyperelastic model, which captures the basic characteristics of passive biomechanical response of the artery, is exponential Fung's SEF (Fung et al. [3]), expressed in the form

$$\begin{aligned} \hat{\psi} &= \frac{1}{2} C [\exp(Q) - 1], \\ Q &= a_1 E_{11}^2 + a_2 E_{22}^2 + 2a_4 E_{11} E_{22}, \end{aligned} \quad (4)$$

where the constant  $C > 0$  is a stress-like material parameter; and  $a_1$ ,  $a_2$ ,  $a_4$  are the non-dimensional parameters. Another 2D SEF for arteries was proposed by Takamizawa and Hayashi [21]. It has a logarithmic form

$$\begin{aligned} \hat{\psi} &= -C \ln(1 - Q), \\ Q &= a_1 E_{11}^2 + a_2 E_{22}^2 + 2a_4 E_{11} E_{22}, \end{aligned} \quad (5)$$

where, as previously, the constant  $C > 0$  is a stress-like material parameter, and  $a_1$ ,  $a_2$ ,  $a_4$  are the non-dimensional parameters. In both cases, the SEFs are convex if the material constants satisfy condition  $a_1 a_2 > a_4^2$ ,  $a_1, a_2 > 0$  (Holzapfel et al. [4]), and this condition also follows from analysis of deformations and normal stresses under planar uniaxial (Veljković and Kojić [24]) and planar constrained biaxial loading (Humphrey [10]).

The SEF proposed by Vaishnav et al. [22] have a polynomial form, and we use here a variant with seven material constants, given by

$$\begin{aligned} \hat{\psi} &= c_1 E_1^2 + c_2 E_1 E_2 + c_3 E_2^2 + c_4 E_1^3 \\ &\quad + c_5 E_1^2 E_2 + c_6 E_1 E_2^2 + c_7 E_2^3 \end{aligned} \quad (6)$$

where  $c_i$ ,  $i = 1, 2, \dots, 7$  are material parameters with dimension of stress. Unfortunately, because of the cubic nature of the SEF (6), it is not convex for any

set of the material parameters (Holzapfel et al. [4]), so that this model may produce unrealistic material behaviour, as already notified in [10] and [24].

A three-dimensional (3D) exponential polyconvex anisotropic (orthotropic and transversely isotropic) SEF suitable for soft biological tissues (Itskov et al. [11]) has the form

$$\psi = \frac{1}{4} \sum_{r=1}^s \mu_r \times \left\{ \frac{1}{\alpha_r} (\exp[\alpha_r(\tilde{I}_r - 1)] - 1) + \frac{1}{\beta_r} (\exp[\beta_r(\tilde{K}_r - 1)] - 1) \right\}, \quad (7)$$

$$\tilde{K}_r = \text{tr}(\mathbf{C}^{-1} \tilde{\mathbf{L}}_r), \quad \tilde{\mathbf{L}}_r = \sum_{i=1}^3 w_i^{(r)} \mathbf{L}_i, \quad (8)$$

$$\tilde{I}_r = \sum_{i=1}^3 w_i^{(r)} I_i, \quad \sum_{i=1}^3 w_i^{(r)} = 1, \quad r = 1, 2, \dots \quad (9)$$

Here  $I_i = \text{tr}(\mathbf{C}\mathbf{L}_i)$  denote deformation invariants for orthotropic hyperelastic material,  $\mathbf{C}$  is the right Cauchy–Green deformation tensor, and  $\mathbf{L}_i$  are structural tensors,  $i = 1, 2, 3$ . Material parameters  $\mu_r$  have dimension of stress;  $\alpha_r, \beta_r$  are dimensionless, as well as the weighting factors  $w_i^{(r)}$ . This SEF a priori satisfies the condition of the energy- and stress-free natural state so that no additional restrictions have to be imposed to material constants (Itskov et al. [11]), unlike previously described 2D models.

It is frequent in the literature that isotropic models are used for modeling an averaged passive biomechanical arterial behaviour. Isotropic 3D SEF proposed by Delfino et al. [2], which is suitable to model typical stiffening effects in the high pressure domain, is given by

$$\psi = \frac{a}{b} \left\{ \exp \left[ \frac{b}{2} (I_1 - 3) \right] - 1 \right\} \quad (10)$$

where  $a > 0$  is a stress-like,  $b > 0$  is a non-dimensional material parameter, and  $I_1 = \text{tr}(\mathbf{C})$  is the first invariant of the right Cauchy–Green deformation tensor.

## 2.2. Methods

We used one porcine aorta resected from a young healthy pig weighing about 20 [kg], stored after removal from the body in Krebs–Ringer solution (KRS), in mM: NaCl 117, KCl 4.7, NaHCO<sub>3</sub> 24.8, MgSO<sub>4</sub> × 7H<sub>2</sub>O 1.2, CaCl<sub>2</sub> 2.5, KH<sub>2</sub>PO<sub>4</sub> 1.2 and D-glucose

11.1 (Merck, Darmstadt), at 4 [°C]. The vessel was placed in a temperature controlled bath filled with oxygenated (95% O<sub>2</sub>, and 5% CO<sub>2</sub>) buffered KRS, maintained at a temperature of 37 ± 0.5 [°C], and all mechanical tests were performed within 8 hours.

The experimental setup shown in Fig. 1 is very similar to that used by Vaishnav et al. [22] and Fung et al. [3]. The one end of the artery segment (5) placed in the temperature controlled bath (4) was connected to a fixed support (7), where a pressure transducer (6) was assembled. The other end of the artery was connected to the arm of balance (11) via a force transducer. Axial stress changes were introduced by a slide mechanism (11, 12) with the digitally controlled DC motor, to which the balance arms were attached. The lumen is perfused with KRS (1), using the first peristaltic pump (2) at 9.5 [ml/min]. The distal part of the specimen was connected to the two-way tap, allowing a change of maximal hydrostatic pressure from 0 to 180 [mm Hg] (heights H<sub>1</sub>, H<sub>2</sub>, ...).

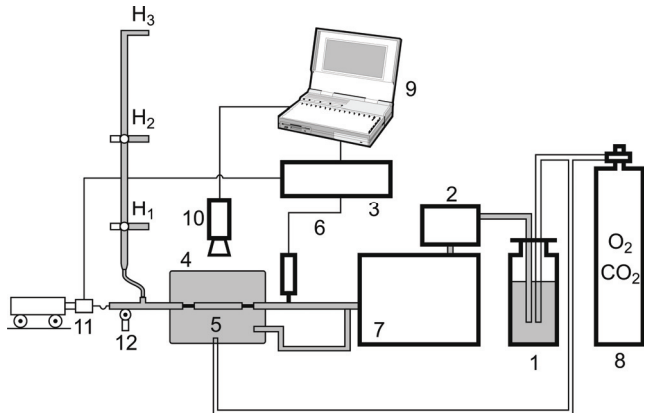


Fig. 1. Schematic representation of the experimental setup for the simultaneous inflation and extension of cylindrical blood-vessel segment.

- (1) Krebs–Ringer solution (KRS); (2) peristaltic pump;
- (3) data acquisition module; (4) temperature controlled bath;
- (5) artery segment (specimen); (6) pressure transducer;
- (7) fixed support; (8) gas mixture; (9) PC; (10) video camera;
- (11), (12) slide mechanism with force transducer

The exterior of the vessel was perfused with KRS maintained at 37 ± 0.5 [°C], from a reservoir (1) using the second peristaltic pump at 3 [ml/min], and aerated with the same gas mixture (8) as the lumen of the artery. The vascular diameter and axial gauge length were sensed optically (10) to avoid any mechanical interference, while the axial force and intraluminal pressure were measured and then digitized with data acquisition module (3). In order to avoid hysteresis effects, the vessel was first preconditioned by repeated inflation to 180 [mm Hg] and deflation

to zero. The five experimental protocols were carried out:

- I. Inflation from 0 to 180 [mm Hg], while one end of artery was able to move freely in axial direction;
- II. Inflation from 0 to 120 [mm Hg] at 10% axial pre-stretch, measured at the specimen fixation points;
- III. Inflation from 0 to 150 [mm Hg] at 28% axial pre-stretch, measured at the specimen fixation points;
- IV. Axial stretching at a constant rate, while intraluminal pressure was maintained at 80 [mm Hg], and
- V. Axial stretching at a constant rate, while intraluminal pressure was maintained at 120 [mm Hg].

Protocols IV and V are slightly different to that made in [22] and [3], where experimental setup allowed only continuous extension with a constant rate at zero intraluminal pressure.

The unstretched vessel wall thickness  $H$  and outer diameter  $D_o$  was determined from the two slices of the distal and proximal ends of the blood vessel, obtained from the specimen after the mechanical testing, and the average values were calculated:

$$H = 1.51 \text{ [mm]}, \quad D_o = 2R_o = 12.67 \text{ [mm]}. \quad (11)$$

Thickness of the vessel wall  $h$  during testing is calculated using the measured values of diameter of the artery  $d_o = 2r_o$ , the current gauge length  $l$ , and incompressibility assumption (Fung et al. [3]), as

$$h = \sqrt{r_o^2 - V/(\pi l)}, \quad (12)$$

where  $V = \pi(D_o - H)HL = \text{const}$  is volume of the observed part of the specimen, between markers in axial direction which defines the initial gauge length  $L$ . The stretch ratios of the blood vessel are obtained from

$$\lambda_\theta = \frac{d_o - h}{D_o - H}, \quad \lambda_z = \frac{l}{L}. \quad (13)$$

Here, the circumferential stretch  $\lambda_\theta$  is calculated at the middle surface of the blood vessel,  $d_o - h$ . The corresponding stresses for a thin-walled cylindrical tube (Holzapfel et al. [4]; Fung et al. [3]) are determined as

$$S_{\theta\theta} = \frac{1}{\lambda_\theta^2} \frac{p_i r_i}{h}, \quad S_{zz} = \frac{1}{\lambda_z^2} \frac{F + p_i r_i^2 \pi}{(r_o^2 - r_i^2) \pi}, \quad (14)$$

where  $\theta$  and  $z$  denote the circumferential and axial direction of the artery, respectively, i.e., directions 1 and 2 in the context of hyperelastic models introduced in the previous section. Here,  $F$  is the measured axial force at the vessel ends,  $p_i$  is the intraluminal pressure,

and  $r_i = r_o - h$  is the inner radius of the artery. The Green–Lagrange strains in the circumferential and axial directions are given by

$$E_{\theta\theta} = \frac{1}{2} (\lambda_\theta^2 - 1), \quad E_{zz} = \frac{1}{2} (\lambda_z^2 - 1). \quad (15)$$

Experimental trajectories of the Green–Lagrange strains in the circumferential and axial direction of the arterial segment, generated during the five inflation-extension experiments performed on the one complete cylindrical segment of porcine aorta, are shown in Fig. 2. Note that for protocol II, when inflation of the specimen is subjected to 10% axial pre-stretch measured at the specimen fixation points, the actual axial stretch  $\lambda_z$  measured in the middle part of the arterial segment, shown in Fig. 2, changes from 14.1% to 23.2%. On the other hand, for protocol III, when axial pre-stretch of the specimen is 28% at fixation points, the axial stretch in the central part changes from 36.5% to 42.3%, due to gripping effects.

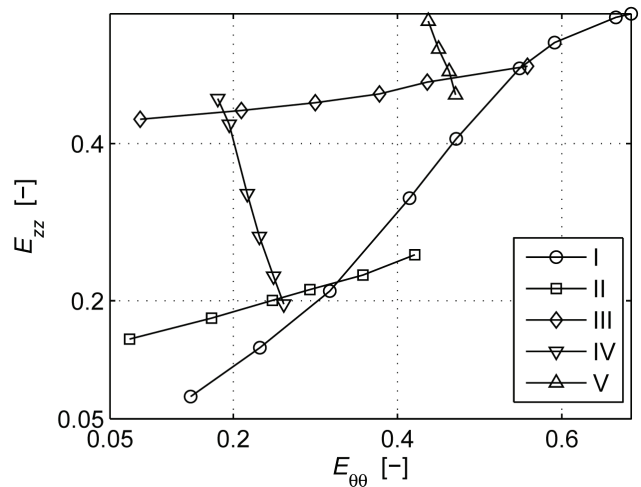


Fig. 2. Experimental trajectories of the Green–Lagrange strains generated during the inflation-extension experiments performed on a cylindrical segment of porcine aorta: I – inflation from 0 to 180 [mmHg], while the one end of the artery was able to move freely in axial direction; II and III – inflation at 10% and 28% axial pre-stretch, measured at the specimen fixation points, respectively; IV and V – axial stretching at a constant rate, while intraluminal pressure was maintained at 80 and 120 [mmHg], respectively

Experimental data of the 2nd Piola–Kirchhoff stresses (14) in axial and circumferential direction of the artery segment versus Green–Lagrange strains (13) in both specimen directions are presented in Fig. 3 and Fig. 4, respectively.

It is well known that each arterial segment shortens after removal from the body, and that in vivo pre-stretch should be reproduced performing in vitro test

(Holzapfel et al. [4]). Our tests are made without this information, but they are designed in such a way that a wide range of physiologically possible deformations are covered by experimental strain paths.

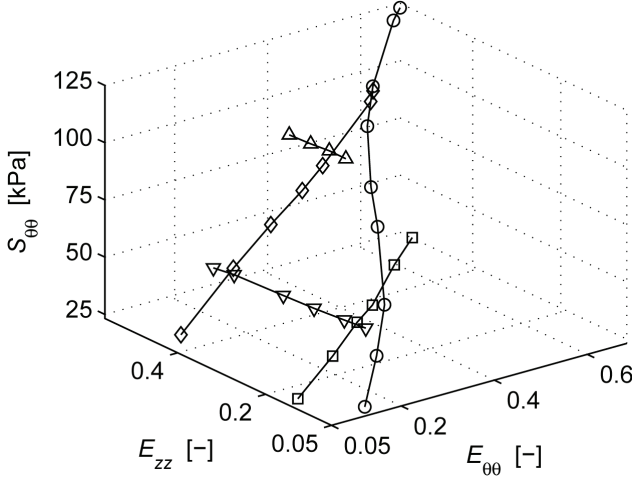


Fig. 3. Experimental data of 2nd Piola–Kirchhoff stresses in axial direction of artery versus Green–Lagrange strains in circumferential and axial specimen direction for all five test protocols

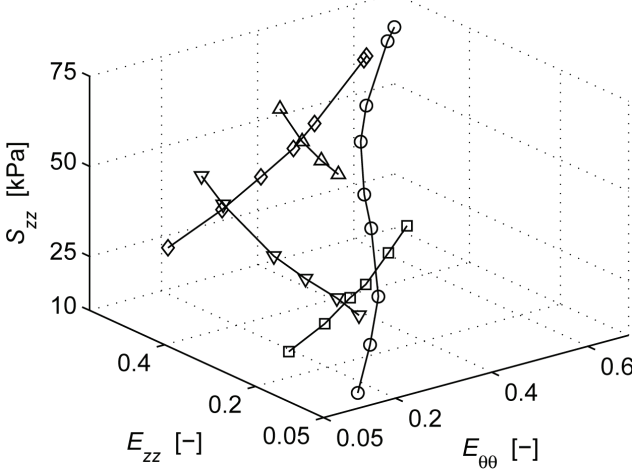


Fig. 4. Experimental data of 2nd Piola–Kirchhoff stresses in circumferential direction of artery versus Green–Lagrange strains in circumferential and axial specimen direction for all five test protocols

### 3. Results

We used the non-linear least squares method for fitting the hyperelastic constitutive laws given in the previous Section: 2D orthotropic models; the polyconvex 3D anisotropic model; and the 3D isotropic exponential rubber-like model, to the experimental data of the five inflation-extensions tests. The objec-

tive function (Ogden et al. [16]) was minimized with respect to the material constants by means of the Nelder–Mead type algorithm (Press et al. [17]) simultaneously for all five protocols. The optimal set of material parameters for Fung's exponential 2D SEF is

$$C = 756.5 \text{ [kPa]}, \quad a_1 = 0.166, \\ a_2 = 0.084, \quad a_4 = 0.045, \quad (16)$$

while for the logarithmic 2D SEF it is

$$C = 512.5 \text{ [kPa]}, \quad a_1 = 0.250, \\ a_2 = 0.126, \quad a_4 = 0.068. \quad (17)$$

We can conclude that both SEFs give good, but not perfect, fit with respect to the experimental data for all experiments considered. Actually, the mean relative errors for the exponential and logarithmic SEF are  $\delta_\theta = 6.4\%$  and  $\delta_\theta = 6.8\%$ , and  $\delta_z = 14.6\%$  and  $\delta_z = 14.1\%$ , respectively. Note that in both cases the optimal material constants are satisfying the condition  $a_1 a_2 > a_4^2$ ,  $a_1 a_2 > 0$ , which is necessary for the SEFs convexity (Holzapfel et al. [4]) to avoid unrealistic material response in the case of the planar uniaxial (Veljković and Kojić [24]) and the planar constrained biaxial loading (Humphrey [10]).

For the polynomial 2D SEF the optimal set of material parameters (in kPa) is

$$c_1 = 52.35, \quad c_2 = 70.14, \quad c_3 = 21.75, \quad c_4 = 3.53, \\ c_5 = 27.50, \quad c_6 = -67.65, \quad c_7 = 28.90. \quad (18)$$

The mean errors  $\delta_\theta = 5.5\%$  and  $\delta_z = 12.5\%$  are slightly lower when compared to the exponential and logarithmic 2D SEFs. But, as already mentioned, this SEF is not convex for any set of material constants. Also, material parameter  $c_6 < 0$ , which, according to Humphrey [10] and Veljković and Kojić [24], leads to unrealistic prediction of stresses and strains in the case of planar uniaxial and constrained biaxial deformation.

The series used for the 3D orthotropic polyconvex SEF (7) has been truncated at the first term ( $s = 1$ ) so that the total number of the unknown material constants was 5, with the fitted values (following from five experiments)

$$\mu_1 = 94.97 \text{ [kPa]}, \quad \alpha_1 = 1.04, \\ \beta_1 = 1.58, \quad w_1^1 = 0.6226, \quad w_2^1 = 0.3767, \quad (19)$$

and  $w_3^1 = 1 - w_1^1 - w_2^1 = 0.007$ . The mean relative errors between experimental and modeled values of stresses in the circumferential and axial directions for this model are:  $\delta_\theta = 5.2\%$  and  $\delta_z = 17.1\%$ . As can be seen, relative error of the stresses in the circumfer-

tial direction is minimal for this SEF compared to other implemented orthotropic 2D SEFs, while it is maximal for the axial direction. The optimal material coefficients for the isotropic rubber-like 3D SEF are obtained as

$$a = 40.12 \text{ [kPa]}, \quad b = 1.074, \quad (20)$$

while the mean relative errors for the stresses are:  $\delta_\theta = 19.0\%$ ,  $\delta_z = 32.1\%$ . As expected, the mean relative errors are significantly higher for the isotropic model than for previously used 2D and 3D orthotropic

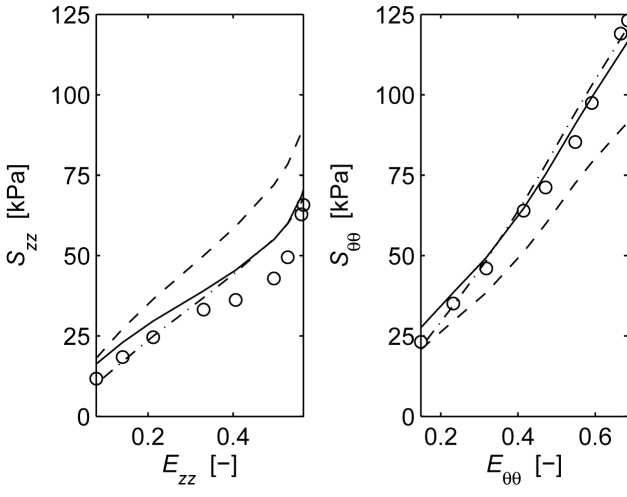


Fig. 5. Experimental data for test I (points)  
and their respective model fits:

orthotropic exponential Fung's 2D model (dash-dot line);  
isotropic exponential Delfino's 3D model (dotted line);  
anisotropic exponential polyconvex Itskov's 3D model (full line)

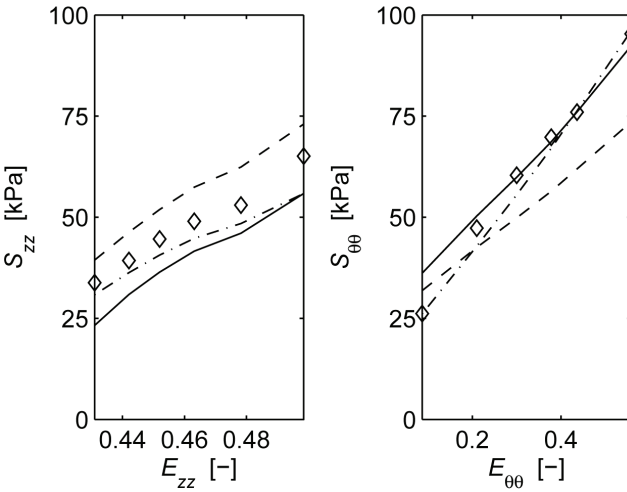


Fig. 6. Experimental data for test III (points)  
and their respective model fits:  
orthotropic exponential Fung's 2D model (dash-dot line);  
isotropic exponential Delfino's 3D model (dotted line);  
anisotropic exponential polyconvex Itskov's 3D model (full line)

models, since the observed porcine abdominal aorta tissue response is significantly orthotropic.

A graphical comparison of the experimental data for protocols I, III and IV, together with the values given by stress-strain relationships corresponding to Fung's orthotropic 2D hyperelastic model (4), Delfino's isotropic 3D hyperelastic model (10), and Itskov's anisotropic hyperelastic 3D model (7) are shown in Fig. 5, Fig. 6 and Fig. 7, respectively. We found that for the logarithmic and polynomial 2D SEFs the results are almost the same as for Fung's model, and they are not included here separately.

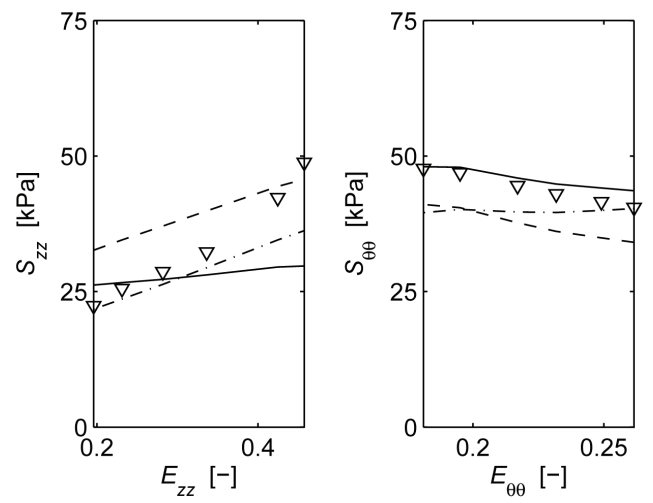


Fig. 7. Experimental data for test IV (points)  
and their respective model fits:

orthotropic exponential Fung's 2D model (dash-dot line);  
isotropic exponential Delfino's 3D model (dotted line);  
anisotropic exponential polyconvex Itskov's 3D model (full line)

By inspecting data in these figures, we can see that the isotropic SEF (10) overestimates the values of stresses in axial direction, and underestimates values of stresses in circumferential direction of artery segment, due to tissue anisotropy. It is interesting that Itskov's polyconvex 3D hyperelastic model (7) gives good and similar prediction of stresses in circumferential direction of artery segment as Fung's 2D model, with slightly poorer performance in the axial direction of artery segment compared with Fung's SEF. Of course, these conclusions should be checked on a greater number of specimens, since the variation in the mechanical properties of tissue samples is rather large, as already mentioned in many studies of the passive biomechanical properties of soft biological tissues (Fung et al. [3]; Takamizawa and Hayashi [21]; Lally et al. [12]).

## 4. Discussion

In this paper, we have presented results of the experimental investigation of the passive hyperelastic biomechanical characteristics of porcine abdominal aorta, with fitting several phenomenological hyperelastic models to these experimental data. Five extension-inflation tests were performed on one porcine aorta segment, including: I – inflation from 0 to 180 [mm Hg], while one end of the artery was able to move freely in axial direction; tests II and III, with inflation giving 10% and 28% axial pre-stretch at the specimen fixation points, respectively; IV and V – axial stretching at a constant rate, while intraluminal pressure was maintained at 80 and 120 [mm Hg], respectively. The latest two experimental protocols are slightly different when compared to those in the literature, where only axial stretching at a constant strain rate were imposed at a zero intraluminal pressure (Vaishnav et al. [22]; Fung et al. [3]). Since it is generally accepted that arterial wall materials are incompressible, a membrane approximation is used to compute stresses and strains. The non-linear least squares method for the minimization of the objective function was implemented in order to identify the optimal material constants for all five tests simultaneously. The three orthotropic 2D SEFs are fitted to the test data: the well-known Fung's exponential model, the classical polynomial model with seven constants, and the logarithmic model. Also the 3D polyconvex orthotropic model (Itskov et al. [11]) and isotropic 3D exponential rubber-like SEF (Delfino et al. [2]) were employed. The mean relative errors in stresses in the circumferential and axial direction were about  $\delta_\theta = 6\%$  and  $\delta_z = 15\%$ , for the orthotropic models; while for 3D isotropic SEF the average errors were much higher:  $\delta_\theta = 19.0\%$  and  $\delta_z = 32.1\%$ , due to arterial tissue anisotropy.

The identified sets of the material constants for several phenomenological hyperelastic constitutive laws presented in this paper, based on the series of the inflation-extensions tests performed in our laboratory, may be useful in the area of mechanical properties and computer simulations of complex problems arising in cardiovascular mechanics, including transluminal angioplasty, abdominal aortic aneurysm treatment, etc. Note that available data in literature, as already mentioned in [4], are obtained from different animals and/or different arteries, which could be inappropriate for making comparisons of using various models in arterial mechanics. Of course, in the case of only one sample tested, values of the estimated material pa-

rameters are just the example ones, but a good starting point for more detailed studies in the future, which should include some of the more sophisticated models incorporating morphological structure of the blood vessel wall, as (Holzapfel et al. [4]).

## Acknowledgements

Support of the Serbian Ministry of Science and Environmental Protection, Projects TR 6209 and OI 144028, is gratefully acknowledged.

## References

- [1] CHOUNG C.J., FUNG Y.C., *Three-dimensional Stress Distribution in Arteries*, J. Biomech. Eng., 1983, 105(3), 268–274.
- [2] DELFINO A., STERGIOPULOS N., MOORE J.E., MEISTER J.J., *Residual strain effects on the stress field in a thick wall finite element model of the human carotid bifurcation*, J. Biomech., 1997, 30(8), 777–786.
- [3] FUNG Y.C., FRONEK K., PATITUCCI P., *Pseudoelasticity of arteries and the choice of its mathematical expression*, Am. J. Psychol., 1979, 237, H620–H631.
- [4] HOLZAPFEL G.A., GASSER C.T., OGDEN R.W., *A new constitutive framework for arterial wall mechanics and comparative study of material models*, J. Elasticity, 2000, 61(1–3), 1–48.
- [5] HOLZAPFEL G.A., *Nonlinear Solid Mechanics*, 2001, reprinted 2007., John Wiley & Sons.
- [6] HOLZAPFEL G.A., GASSER T.C., OGDEN R.W., *Comparison of a Multi-Layer Structural Model for Arterial Walls with a Fung-Type Model, and Issues of Material Stability*, J. Biomech. Eng., 2004, 126(2), 264–275.
- [7] HOLZAPFEL G.A., OGDEN R.W., *On planar biaxial tests for anisotropic nonlinearly elastic solids. A continuum mechanical framework*, Mathematics and Mechanics of Solids, 2008, 14, 474–489.
- [8] HOLZAPFEL G.A., OGDEN R.W., *Constitutive modeling of arteries*, Proc. R. Soc. A, 2010, 466, 1551–1597.
- [9] HUMPREY J.D., *Mechanics of the arterial wall: review and directions*, Crit. Rev. in Biomed. Engr., 1995, 23, 1–162.
- [10] HUMPREY J.D., *An Evaluation of Pseudoelastic Descriptors Used in Arterial Mechanics*, J. Biomech. Eng., 1999, 121, 259–262.
- [11] ITSKOV M., EHRET A.E., MAVRILAS D., *A polyconvex anisotropic strain-energy function for soft collagenous tissues*, Biomech. Model. Mechanobiol., 2006, 5, 17–26.
- [12] LALLY C., REID A.J., PRENDERGAST P.J., *Elastic Behavior of Porcine Coronary Artery Tissue under Uniaxial and Equibiaxial Tension*, Ann. Biomed. Eng., 2004, 32(10), 1355–1364.
- [13] MARRA S.P., KENNEDY F.E., KINKAID J.N., FILLINGER M.F., *Elastic and Rupture Properties of Porcine Aortic Tissue Measured Using Inflation Testing*, Cardiovasc. Eng., 2006, 6, 125–133.
- [14] MOONEY M.A., *A theory of large elastic deformation*, J. Appl. Phys., 1940, 11, 582–592.
- [15] OGDEN R.W., *Non-Linear Elastic Deformation*, Dover Publications, New York 1997.
- [16] OGDEN R.W., SACCAMONDI G., SQURA I., *Fitting hyperelastic models to experimental data*, Computational Mechanics, 2004, 34, 484–502.

- [17] PRESS W.H., FLANNERY B.P., TEUKOLSKY S.A., VETERLING W.T., *Numerical Recipes. The Art of Scientific Computing*, Cambridge University Press, New York 1986.
- [18] RAGHAVAN M.L., VORP D.A., *Toward a biomechanical tool to evaluate rupture potential of abdominal aortic aneurysm: identification of a finite strain constitutive model and evaluation of its applicability*, J. Biomech., 2000, 33(4), 475–482.
- [19] RIVLIN R.S., SAUNDERS D.W., *Large Elastic Deformations of Isotropic Materials. VII. Experiments on the Deformation of Rubber*, Phil. Trans. Roy. Soc. London, 1951, 243(865), 251–288.
- [20] SACKS M.S., *Biaxial Mechanical Evaluation of Planar Biological Materials*, J. Elasticity, 2000, 61, 199–246.
- [21] TAKAMIZAWA K., HAYASHI K., *Strain Energy Density Function and Uniform Strain Hypothesis for Arterial Mechanics*, J. Biomech., 1987, 20(1), 7–17.
- [22] VAISHNAV N.R., YOUNG J.T., JANICKI J.S., PATEL D.J., *Non-linear Anisotropic Elastic Properties of the Canine Aorta*, Biophys. J., 1972, 12(8), 1008–1027.
- [23] VANDE GEEST J.P., SACKS M.S., VORP D.A., *The effects of aneurysm on the biaxial mechanical behaviour of human abdominal aorta*, J Biomech., 2006, 39, 1324–1334.
- [24] VELJKOVIĆ D.Ž., KOJIĆ M., *Prediction of Planar Uniaxial and Constrained Biaxial State of Deformation by Commonly Used Anisotropic Constitutive Models in Arterial Mechanics*, J. Serb. Soc. Comp. Mech., 2010, 4(2), 54–74.
- [25] VELJKOVIĆ D.Ž., *Simulation of passive biomechanical behaviour of arterial walls by using hyperelastic material models*, PhD Thesis, University of Kragujevac, Kragujevac, Serbia 2012 (in Serbian).